

Article

## Analysis of Incidence Angle and Distance Effects on Terrestrial Laser Scanner Intensity: Search for Correction Methods

Sanna Kaasalainen <sup>1,\*</sup>, Anttoni Jaakkola <sup>1</sup>, Mikko Kaasalainen <sup>2</sup>, Anssi Krooks <sup>1</sup> and Antero Kukko <sup>1</sup>

<sup>1</sup> Department of Remote Sensing and Photogrammetry, Finnish Geodetic Institute, Geodeetinrinne 2, FI-02431 Masala, Finland; E-Mails: Anttoni.Jaakkola@fgi.fi (A.J.); Anssi.Krooks@fgi.fi (A.K.); Antero.Kukko@fgi.fi (A.K.)

<sup>2</sup> Department of Mathematics, Tampere University of Technology, P.O. Box 553, FI-33101 Tampere, Finland; E-Mail: Mikko.Kaasalainen@tut.fi

\* Author to whom correspondence should be addressed; E-Mail: Sanna.Kaasalainen@fgi.fi; Tel.: +358-9-2955-5203; Fax: +358-9-2955-5200.

Received: 23 August 2011; in revised form: 3 October 2011 / Accepted: 12 October 2011 /

Published: 20 October 2011

---

**Abstract:** The intensity information from terrestrial laser scanners (TLS) has become an important object of study in recent years, and there are an increasing number of applications that would benefit from the addition of calibrated intensity data to the topographic information. In this paper, we study the range and incidence angle effects on the intensity measurements and search for practical correction methods for different TLS instruments and targets. We find that the range (distance) effect is strongly dominated by instrumental factors, whereas the incidence angle effect is mainly caused by the target surface properties. Correction for both effects is possible, but more studies are needed for physical interpretation and more efficient use of intensity data for target characterization.

**Keywords:** terrestrial laser scanning; intensity; radiometric calibration; incidence angle

---

### 1. Introduction

The signal received by a LiDAR detector is mainly affected by four essential factors: instrumental and atmospheric effects, the target scattering characteristics, and the measurement geometry. The radar

equation summarizes all the parameters relevant to describe these effects and the power of the backscattered signal in a laser scanner detector [1]. The equation can be expressed in a form suitable for LiDAR systems as [2]:

$$P_r = \frac{P_t D_r^2}{4\pi R^4 \beta_t^2} \sigma \quad (1)$$

where  $P_r$  is the received power,  $P_t$  is the transmitted power,  $D_r$  is the receiver aperture,  $R$  is the range, and  $\beta_t$  is the transmitter beam width.  $\sigma$  is the backscatter cross section: it describes the scattering of a wave from an object. The backscatter cross-section  $\sigma$  is related to the illuminated target area: as the range increases, also the illuminated area and the backscatter cross-section increase with respect to  $R^2$ . Therefore the power of the backscattered signal is inversely proportional to  $R^2$  for homogeneous targets spreading over the entire laser footprint (these are called extended targets [1]). For linear objects and individual large scatterers, the intensity is proportional to  $R^3$  and  $R^4$  respectively [1,2].

In addition to the target scattering properties and atmospheric and instrumental parameters, the backscattered signal is affected by the scanning geometry, particularly the range (distance) and the beam incidence angle to the target. In terrestrial laser scanning (TLS), where the target surface is most often larger than the laser footprint size, the case for extended targets can be considered, and the range dependence can be expressed in terms of  $1/R^2$ , where  $R$  is the range.

While numerous studies on airborne laser scanning (ALS) intensity calibration have become available recently [2-6], studies of TLS radiometric calibration are still sparsely available. Range effects on the TLS intensity have been studied by, e.g., comparing two different scanners with respect to diffuse reflectance standards [7]. Different results for different scanners were obtained and a data-driven model was introduced. The effect of partly overlapping footprints in TLS systems was studied for the Optech ILRIS 3D, whereas there was no explanation for the complicated intensity vs. distance behavior for the Riegl LMS-Z420i scanner. Applications that use distance-normalized intensity data have been presented in vegetation studies for mapping leaf area distribution [8] and in geology, e.g., for the discrimination of different rocks, and for the investigation of outcrop lithology or surface patterns (such as moisture and roughness) [9-11].

Knowing the instrumental effects on the intensity measurement, such as whether there are logarithmic amplifiers for small reflectance or near-distance reducers, is important in the study of distance effects on TLS intensity [12-15]. Only then is it possible to search for a distance correction that would work for different instruments. In addition to the detector itself, the data processing software may introduce some further normalizations at any stage of the data exportation or processing that actually cause losses of intensity information. For example, the Leica Cyclone 7.1 software automatically applies arbitrary scaling of the intensity data, to, e.g., improve the visual appearance [13,16,17]. Using an alternative (Zoller & Fröhlich) software this problem can be avoided, and the intensity scale becomes linear [13]. Therefore it is important to recognize the possible instrumental effects from the data. This can be done with the aid of a reference scale with known reflectance values (such as a multi-step reference target or another pre-calibrated grayscale).

The incidence angle has an effect on data quality. The laser footprint increases significantly as the incidence angle increases [14,18]. Normal incidence is recommended [19] but this is not always possible, especially in mobile TLS applications (e.g., [20,21]). The calibration of flat targets such as

painted tarps has proven to be more straightforward (in practice, these are targets with a smooth surface with respect to the laser footprint or spot size, even though they are still rough with respect to the laser wavelength), and produces a reasonable accuracy [7,22,23]. More studies are needed for surfaces with increasing irregularity, because those surfaces do not follow the Lambertian scattering law. The role of specular reflections should also be studied in more detail [24]. An empirical approach was presented in [14] for leaf surfaces, but it has been found that there is little variation with the incidence angle in the backscattered signal from an irregular surface [19]. Macroscopic irregularities (in mm to cm scale, *i.e.*, the scale of the laser footprint) neutralize the incidence angle effect on intensity, because there are always elements in the surface that are perpendicular to the incident beam. The intensity effect was stronger in the case of the most reflective material [19]. Therefore, the possible correction for incidence angle effects should also include information on the target surface reflectivity.

The aim of this study is to analyze the distance and incidence angle effects in TLS data along with the development of practical correction methods for the intensity data. We also investigate the possibility to relate the TLS intensity *vs.* incidence angle data to surface roughness and grain properties. The surface roughness and grain size play a crucial role in surface characterization, e.g., in fluvial studies [21,25] or glaciology, where these parameters are needed in the interpretation of, e.g., radar based snow cover remote sensing [26,27]. Large-scale grain roughness has been studied from TLS data to retrieve surface structure information for river morphology [25]. In our previous studies, we have investigated the radiometric calibration of TLS intensity [13], and the incidence angle and distance effects on the intensity [12,22,28]. In this paper we have combined our knowledge on these effects, and search for a correction procedure that could be adapted for most TLS instruments and targets. The paper is organized as follows: the data and samples are presented in Section 2. The results are presented in Section 3. Discussion and conclusions are provided in Sections 4 and 5, respectively.

## 2. TLS Data and Samples

The TLS data analyzed in this paper have been combined from our previous studies [13,22,28]. New measurements using a Sick LMS151 have also been included. Table 1 provides an overview of the data, instruments, and samples used in this study.

**Table 1.** Summary of measurements, instruments (see also Table 2 for details), and samples. One new gravel sample (concrete sand) has been added to the incidence angle study.

Data	Instrument (see Table 2)	Reference	Samples
Intensity <i>vs.</i> range	FARO LS 880HE80	[13]	4-step Spectralon target
Intensity <i>vs.</i> range	Leica HDS 6100	[13]	4-step Spectralon target
Intensity <i>vs.</i> range	Sick LMS151	New data	4-step Spectralon, brightness tarps
Intensity <i>vs.</i> incidence angle	FARO LS 880HE80	[28]	Brightness tarps, sand & gravel

**Table 2.** Specifications for the TLS instruments used in the experiments. The Sick LMS 151 field of view is horizontal.

	<b>FARO LS 880HE80</b>	<b>Leica HDS6100</b>	<b>Sick LMS151</b>
Wavelength	785 nm	650–690 nm	905 nm
Unambiguity range	76 m	79 m	50 m
Field-of-view	360° × 320°	360° × 310°	270°
Beam diameter	3 mm	3 mm	8 mm
Beam divergence	0.25 mrad	0.22 mrad	15 mrad

The aim of this study is to compare the new data (obtained with the Sick LM151 scanner) with previously published experiments with FARO LS 880HE80 and Leica HDS 6100 scanners [13] (see Table 1 for a summary of measurements and data), and also to study whether a correction method based on the radar equation is possible, which would be independent on the instrument or target.

Both FARO and Leica scanners are phase-based (continuous wave) laser scanners, see Table 2 for scanner parameters. Measurements with both instruments have been carried out in a similar way: the target has been moved away from the scanner, and the intensity of the target has been measured either in stationary scanning mode or extracted from the profiler mode at 0.5–1 m increments (see [13] for more details). A four-step Spectralon® (Labsphere Inc.) [29] calibrated reference panel with 12%, 25%, 50%, and 99% nominal reflectance has been used as a target in the distance measurements. There is a logarithmic amplifier for low intensities in the FARO scanner, which required an additional correction for the intensity scale [12]. The average errors for the intensity measurements with FARO and Leica are also presented in [13], and are typically of order 1%–5%. The intensity is sampled by averaging over all points in a selected surface area in the laser point cloud (with the aid of the intensity image), and the standard deviation of this average represents the error limits.

In addition to the phase-based laser scanners, a pulse-based Sick LMS151 2D laser scanner was tested for distance effects (see Table 2 for scanner parameters). The four-step Spectralon® and painted polyester tarp targets (of 50%, 26%, 16% and 6% reflectance) were used in the measurements. The polyester tarp samples have been used as reference targets in our previous studies of ALS and TLS radiometric calibration, and described in more detail in [12]. The tarps have smooth matte painted surfaces for optimized reflectance properties (e.g., to minimize specular reflections). Because of the large beam divergence (15 mrad) and laser footprint of the scanner, and the size of the panels (about 115 mm in width), the Spectralon target could only be measured up to a distance of about 9 m. Similarly to FARO and Leica, the intensity was sampled over a selected set of neighboring points with an average error up to 2%. The measurements were corrected for the logarithmic nonlinearity of the instrument by applying the method proposed in [12] before any further analysis was carried out.

Most of the incidence angle measurements have been presented previously in [28]. Results for a concrete sand sample have been added in this paper. In this study, the incidence angle effect is further analyzed and an empirical correction scheme is introduced. The incidence angle measurements have been carried out with the FARO scanner with the measurement error of about 2% [28]. Similarly to the distance measurements with FARO and Leica, the intensity was sampled by averaging over a surface area on a target. The tarp samples were the same ones that were used in the distance experiment with

the Sick LMS151 scanner. Tarps with 70%, 50%, 26%, 16%, and 8% reflectance have been included in the incidence angle study. The gravel samples used in the incidence angle experiment are commercially available sand (used in, e.g., gardening, sandblasting, or for making concrete) and crushed redbrick. The samples included sandblasting sands with grain sizes of 0.1–0.6 mm and 0.5–1.2 mm, concrete sand with grain size varying from 1–5 mm, black gabbro with grain size 2–5 mm, and crushed redbrick with some 10–20 mm grain size. The reflectance values for these samples were approximately 25% for the sands, 9% for the gabbro, and 30% for the crushed redbrick sample. All these were available in standard hardware stores. More detailed information on the gravel samples is available in [4].

### 3. The Distance and Incidence Angle Effects

#### 3.1. The Distance Effect

The distance effect for FARO and Leica is presented in Figure 1 for the four-step Spectralon<sup>®</sup> reference panel. To compare more easily the intensity vs. distance behavior of the two scanners, data have been normalized to equal 1.0 at 12-m distance. Both FARO and Leica detectors are equipped with a brightness reducer for near distances. According to the manufacturer (Zoller+Fröhlich GmbH), the Leica intensity mainly is a function of the receiver optics below distances of about 12 m. The detector effects at distances less than 10 m are clearly visible in the intensity data in Figure 1: they appear, e.g., as deviation in the data and strong decrease in intensity towards zero distance. Comparison with our previous experiments with sand and gravel [13] shows that the distance effect for sand and gravel samples seems to be similar to that for the Spectralon targets presented in this paper. The distance effect also appears to be similar for both scanners (FARO and Leica), at least at distances greater than 10 m, so it is possible to compare the intensity with the  $1/R^2$  prediction from the radar equation. The  $1/R^2$  intensity vs. distance relation has also been discussed in [9].

Assuming that all variables in the radar equation (Equation (1)) are constant, except distance from the target, and that the target fills the whole area of a laser footprint, we can reduce the radar range equation to (*cf.* [30]):

$$P_r = \frac{K}{R^2} \quad (2)$$

where  $K$  is a constant and combines the variables  $P_t$ ,  $D_r$ , and  $\beta_t$ . Apparently, the intensity vs. distance graphs follow the  $R^2$  factor (*cf.* Equation (2)), but they must be scaled with a constant value. This means that the intensity values are somewhat affected by the instrument even at longer distances. Because there are detector effects at the entire range scale, the most suitable means of distance correction is to use a reference table, *i.e.*, correction values determined by reference measurements [13] (also *cf.* [31]).

The Sick LMS151 data, corrected for logarithmic nonlinearity (similarly to FARO, see [12]), are shown in Figure 2. The results show that the intensity response of the instrument is not purely logarithmic. The response of the brighter targets seems to decrease more rapidly at distance from 5 to 10 m, and less rapidly at distances greater than that. Also, at the lower end of the measurable intensity scale, the response is weaker than expected, e.g., the 13 % tarp at distances between 15 and 25 m and 21 % tarp at 22 to 35 m.

**Figure 1.** Intensity vs. range for FARO LS880 and Leica HDS 6100 scanners for the 4-step Spectralon® target, normalized to equal 1.0 at 12 m. The measurement errors (typically 1%–5%) are approximately the same size as the plot symbols. Up to 10 m, the values do not follow the  $1/R^2$  prediction (Equation (2)). The large values near 0 m distance are caused by system noise always present at near-distance measurements.

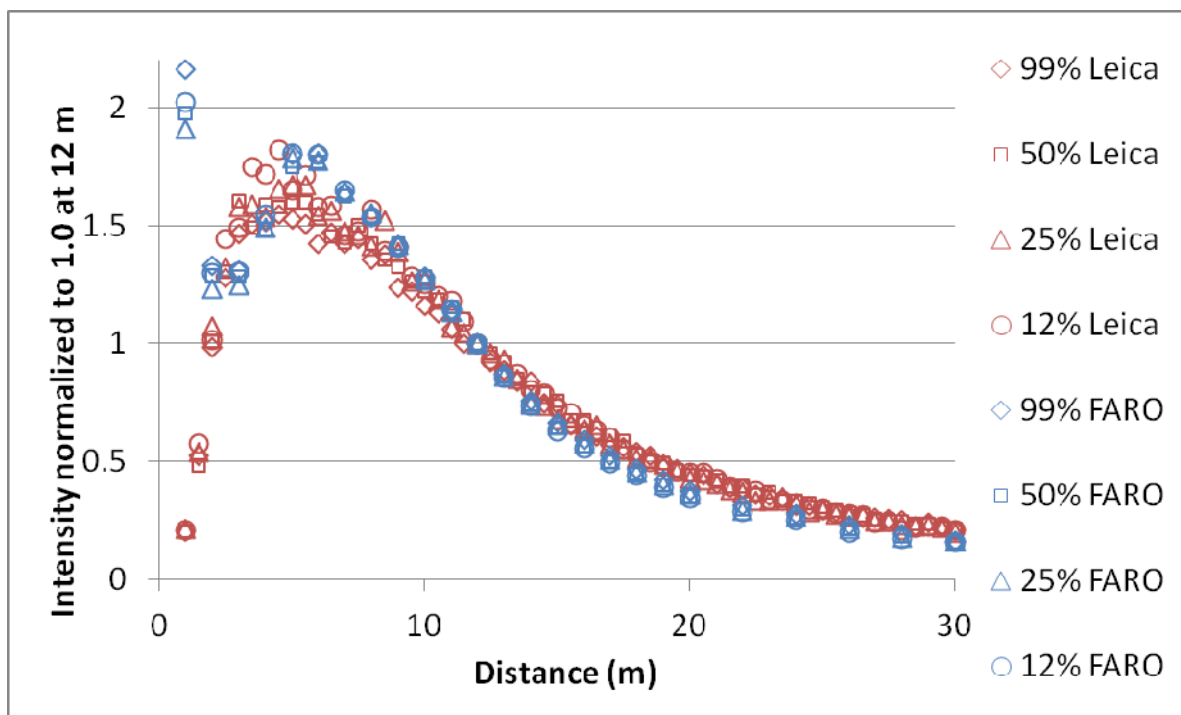


**Figure 2.** Sick LMS151 intensity vs. distance data for brightness tarps (normalized to 1.0 at 12 m (top) and for the 4-step Spectralon® with tarps, normalized to 1.0 at 5 m (bottom)). All data have been corrected for logarithmic behavior.

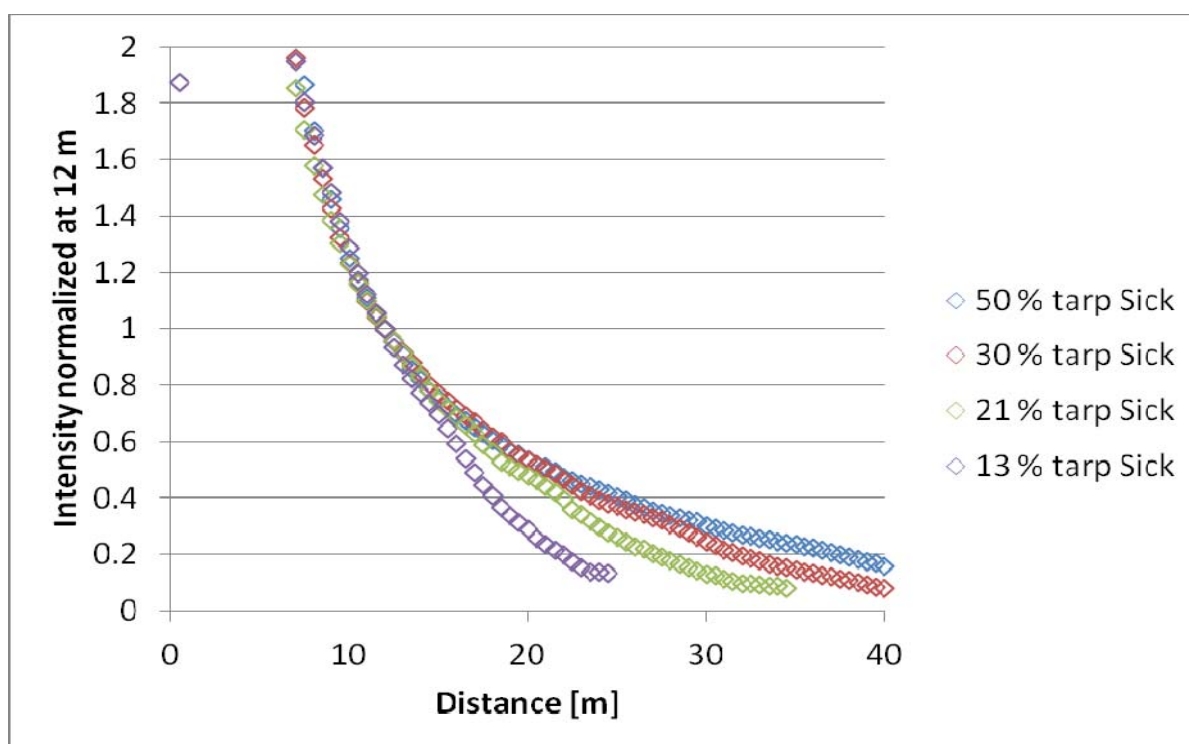
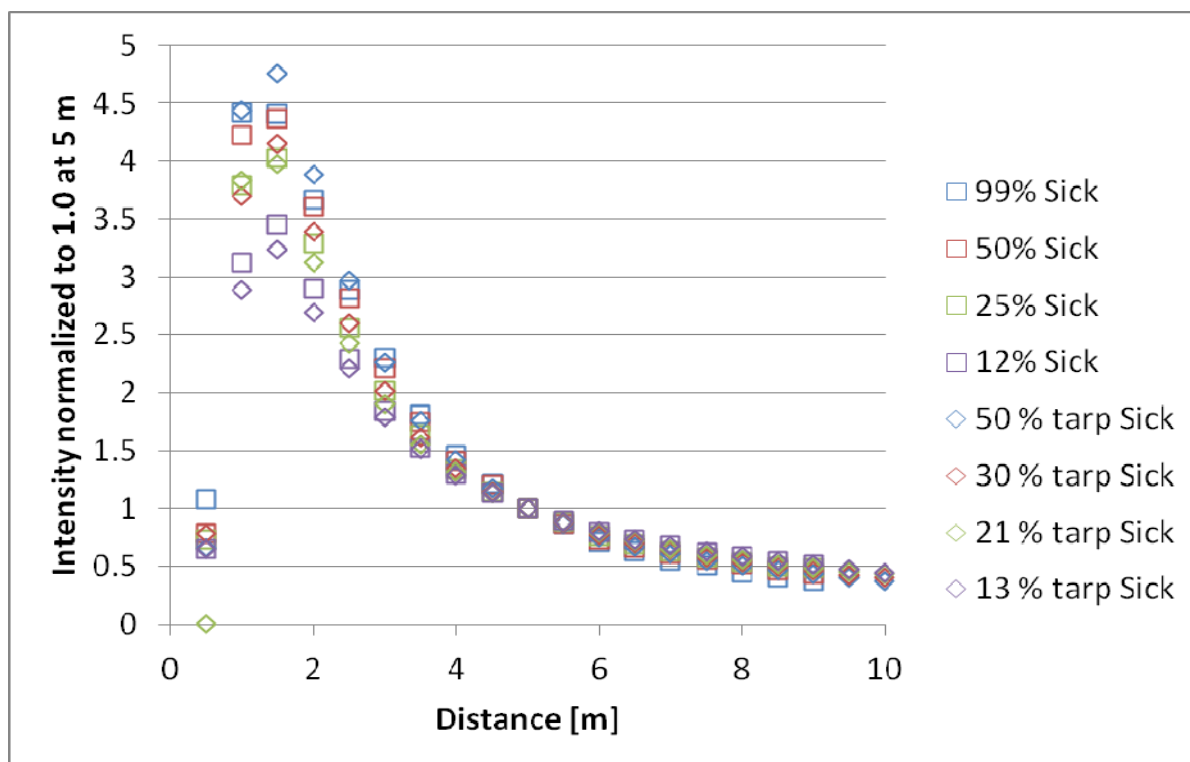


Figure 2. Cont.

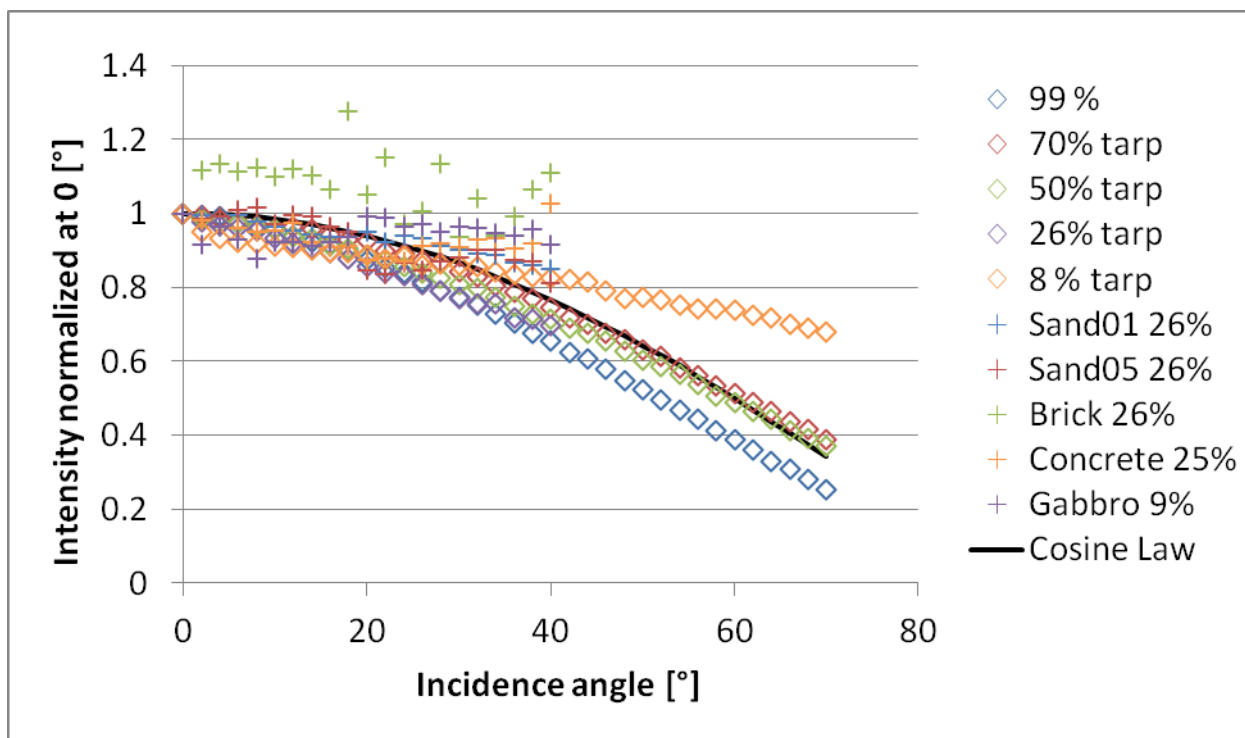


### 3.2. The Effect of Incidence Angle

The effect of incidence angle on the intensity of tarp and sand (gravel) targets is presented in Figure 3. To compare the different targets and the Lambertian (cosine) scattering law, all results have been normalized to  $I(0^\circ) = 1$ . While the intensity trend for the bright targets (such as the 70% tarp) is close to Lambert's law (*cf.* [22]), non-lambertian behaviour occurs for sand and gravel targets, as well as for tarps with lower reflectance. Also, the incidence angle behavior of black gabbro and crushed redbrick appear to be most different from the Lambertian (cosine) scattering law. These targets also have the largest grain sizes. This means that the effect, and hence the correction is related to the surface albedo (reflectance) and the macroscopic surface roughness or grain size of the target. Although the mineralogy of the samples is probably correlated with the data, we first concentrate on the effect of the specific physical properties (*i.e.*, albedo and grain size) of the materials on the measured intensity. It has been found that different intensity response is observed for different rock types [9]. The differences in mineralogy are an important future issue.

In general, any scattering model  $S$  is dependent on the illumination and viewing geometry, *i.e.*, the emergent and incident angles  $\varepsilon, \iota$  and the azimuthal angle between them (*cf.* [32]), and the characteristics of the scattering material. With a suitable experiment setup, we can reduce the model to a simpler special case. The typical experiment carried out here is carried out in exact backscattering, so  $\varepsilon = \iota$  is the only variable describing the illumination and viewing geometry.

**Figure 3.** The effect of incidence angle on the intensity measured with the FARO scanner [28]. To compare the different targets and the Lambertian (cosine) scattering law, all results have been normalized to  $I(0^\circ) = I$  (see also [22]).



As a first approximation, we can take our empirical scattering model to be a combination of the type successfully used in, e.g., space remote sensing [33,34]. This is a linear combination of the Lommel-Seeliger law pertaining to intrinsically dark surfaces and the Lambert law related to brighter targets. Thus we write the scattering law as:

$$S(\varepsilon, \iota) = \cos \varepsilon \cos \iota \left( 2c \frac{1}{\cos \varepsilon + \cos \iota} + d \right) \tag{3}$$

where  $c, d$  are parameters describing the properties of the surface. Since  $\varepsilon = \iota$  in the geometry used here, this actually reduces simply to the first two terms of a power-series expansion, so we do not even need any particular physical derivation, and can consider this fully acceptable for an empirical approach:

$$S(\varepsilon) = c \cos \varepsilon + d \cos^2 \varepsilon \tag{4}$$

In our experiment, the illuminated and viewed area of the planar target surface always gives the same projected area in the viewing direction (see Figure 4 for the experiment setup), so the projection factor  $\cos \varepsilon$  cancels out as the laser beam cross-section  $A$  yields a spot area  $A/\cos \varepsilon$  on the target surface. Thus the observed intensity in our experiment is, in this model,

$$I(\varepsilon) = A(c + d \cos \varepsilon) \tag{5}$$

The parameters  $c, d$  are taken, in the first hypothesis, to be dependent on the reflectance or albedo  $\omega$  of the surface, and the grain size  $g$  of the material. It is advantageous to write Equation (5) in the form

$$I(\varepsilon) = a(\omega, g)(1 - b(\omega, g)(1 - \cos \varepsilon)) \tag{6}$$

where  $a = A(c + d)$  and  $b = d/(c + d)$ . Thus  $I(0) = a$ , and  $b = 0$  represents no Lambertian component, while  $b = 1$  gives a fully Lambertian behavior. Note that  $a(\omega, g)$  is, by definition, directly proportional to  $\omega$ , but it also includes effects such as the backscattering surge (related to the measurement geometry, *cf.* [35]), so the intensities  $I(0)$  are not necessarily directly usable for comparing the ratios of  $\omega$  between various targets.

**Figure 4.** The Incidence angle experiment: The sample placed on a goniometer (left), which is tilted to change the angles of incidence (and emergence). The FARO scanner looking down to the sample (right).



When  $a$  and  $b$  are derived from data, a negative value of  $b$  implies the unphysical case of a negative value of  $d$ , *i.e.*, intensity increasing with  $\varepsilon$ . In the fitting procedure, this means some errors in the experimental data, and  $b = 0$  in practice. A value of  $b > 1$  (negative  $c$ ) implies scattering less diffuse (more specular) than Lambert's: the fitting procedure tries to compensate for the case of intensity decreasing faster than  $\cos(\varepsilon)$ . If  $b$  is much larger than 1, the model should include higher-order terms of  $\cos(\varepsilon)$ , corresponding to a more "peaked" or limb-darkening scattering than the idealized Lambertian case.

The model in Equation (6) fits our experimental data from various targets quite well, as can be seen from Figure 5. We computed the best least-squares fits of  $c, d$  to the observed intensities  $I(\varepsilon)$ , scaled against observed  $I(0) = 1$  set for the 99% Spectralon target, (so that  $A$  cancels out, enabling direct comparison of different experiments), which yielded the  $a, b$  values presented in Table 3.

**Figure 5.** The model in Equation (6) (solid lines) fitted to the experimental incidence angle data. The intensities  $I(\alpha)$  measured with FARO have been divided by the intensity value  $I(0^\circ)$  for the 99% Spectralon, measured similarly to the target (the 99% Spectralon itself was normalized to  $I(0^\circ) = 1$ ).

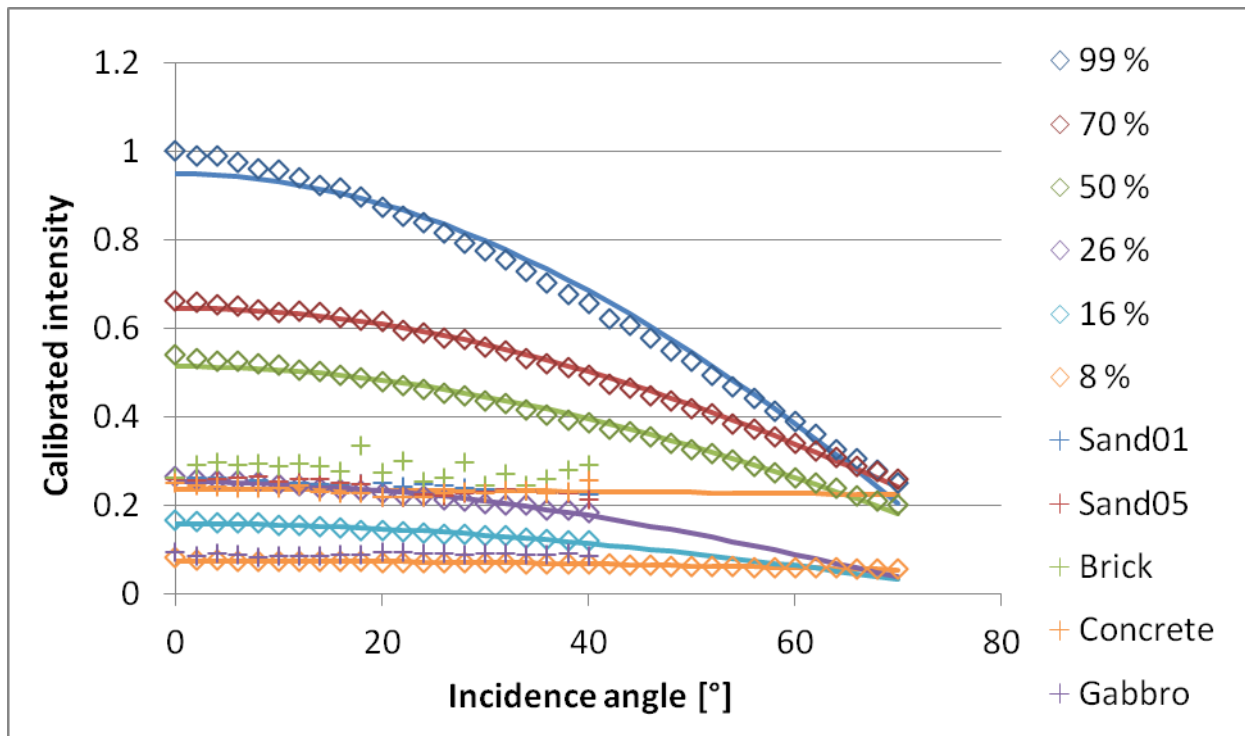


**Table 3.** Parameters  $a, b$  of the correction model (Equation (6)) for each target. Grain sizes for the sand/gravel targets are also included. The relative model fit (root-mean-square, RMS) for the samples was 1%–4%, except 7% for brick, for which there was large inaccuracy in data.

Target	$a$ in Equation (6)	$b$ in Equation (6)
Spectralon 99%	0.95	1.19
Tarp 70%	0.65	0.95
Tarp 50%	0.51	0.98
Tarp 26%	0.25	1.29
Tarp 16%	0.16	1.19
Tarp 8%	0.076	0.42
Sand (0.1–0.6 mm)	0.26	0.59
Sand (0.5–1.2 mm)	0.26	0.71
Concrete sand (1–5 mm)	0.24	0.08
Gabbro (2–5 mm)	0.09	-0.06
Crushed Brick (10–20 mm)	0.29	0.37

While the expression of the dependence on  $\epsilon$  in Equation (6) is apparently reasonably adequate at least as a first approximation, the interpretation of the determined  $b(\omega, g)$  is more complicated. For all

tarp measurements, the compositions of the surfaces were apparently identical at least down to microscopic size [35], so one would expect a monotone sequence of decreasing  $b$  as  $\omega$  (*i.e.*,  $a$ ) decreases. This is clearly not the case as only the darkest tarp behaves as expected. Thus, for the tarps,  $b$  is apparently a much more complicated function of some surface properties that are not immediately manifest. On the other hand, tarps do not fall into the category of particulate surfaces. The samples of such materials behave as expected in that coarse-grained targets have much lower  $b$  values than smooth tarps at similar levels of  $\omega$  (or  $a$ ), similar results were observed with concrete against sand. On the other hand, the  $b$  order of the sand samples (at the same  $a$ ) with respect to their  $g$  values is reverse to the expected one. The results show that systematic experiments at controlled values of albedo ( $\omega$ ) and grain size ( $g$ ) (holding one constant while changing the other) are needed to understand better the relation between surface properties and the incidence angle effect. In the meantime, Equation (6) can be used in the correction of incidence angle effects in TLS data for materials for which  $b$  has been determined.

#### 4. Discussion

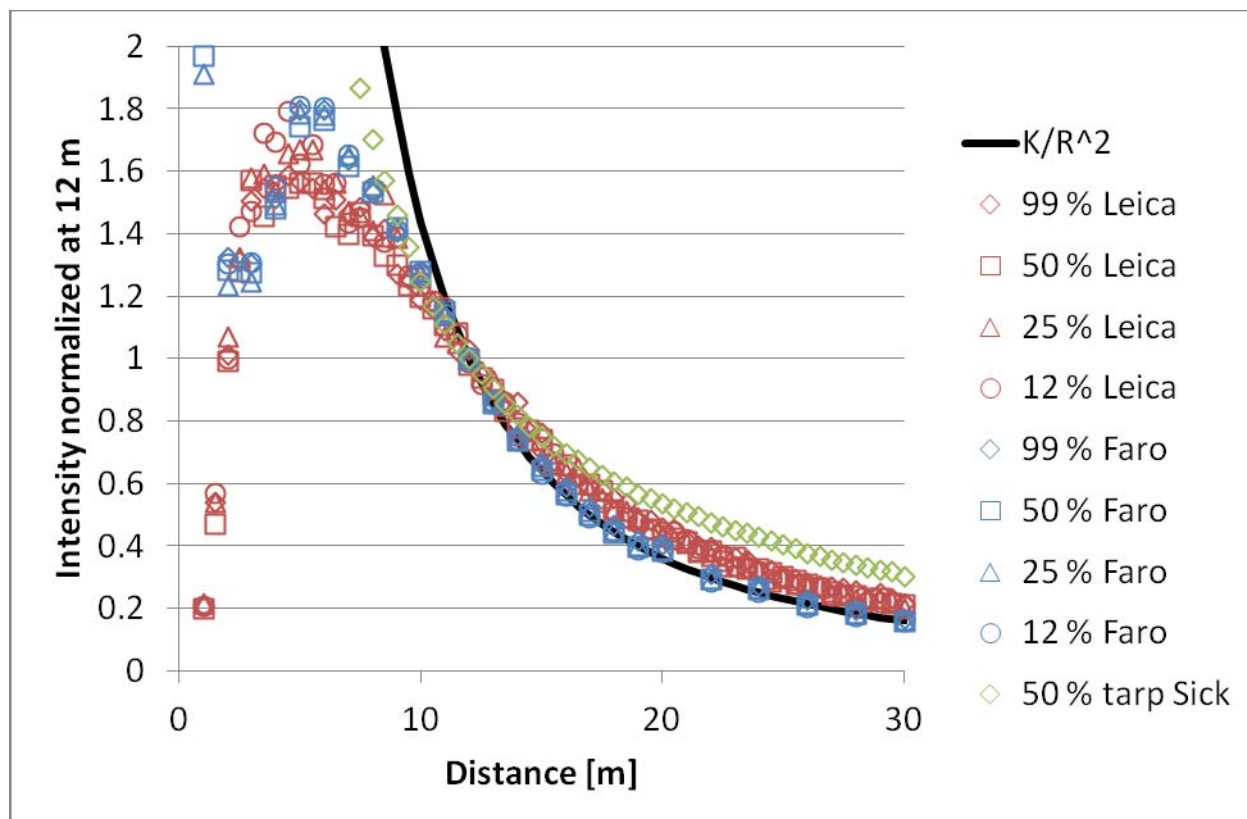
The distance effect was found to be similar with both FARO and Leica scanners. It was also found to roughly follow the  $K/R^2$  prediction (Equation (2)) from the LiDAR equation at ranges of 10–15 m and further (see Figure 6), but the intensity values may need to be scaled with a constant or an offset may have to be added for more accurate results. This means that, if no reference data are available for a reference table correction at long distances, the  $K/R^2$  function could be used in correction, but the constant  $K$  must be determined empirically. The  $K/R^2$  function was also used in [30] for correcting the intensity vs. distance data from the SwissRanger SR-3000 range camera. The results appear to be alike to both FARO and Leica: the  $1/R^2$  correction needed some scaling for the intensity levels to be reproduced.

The near-distance intensity of both FARO and Leica data deviate strongly from the LiDAR equation. A similar result was obtained for the Sick LMS151 scanner, for which the deviation is even stronger. The effect of partly overlapping footprints in TLS systems is discussed in [7], where the emitter and detector are separated. However, the scanners used in this study, *i.e.*, (FARO and Leica) are coaxial and the decrease in intensity at distances less than 5 meters is most likely due to other effects, such as a brightness reducer for small distances (*cf.* [12]).

The interpretation of the incidence angle effect in terms of target surface properties is a complicated task. The results show that more measurements at controlled values of albedo ( $\omega$ ) and grain size ( $g$ ) are needed. This calls for a systematic experiment with well-defined targets, preferably at multiple wavelengths. Wavelength effects (such as offsets in the brightness levels) were observed in our previous experiments of incidence angle effects using a hyperspectral source [28], but the overall brightness trends with the incidence angle were reproduced. Grain size and wavelength relations are discussed in the context of light scattering theories (e.g., [32]), but there is still a great need for systematic study on wavelength effects in practical applications, especially related to the target grain size. Furthermore, future studies will show whether the distance and incidence angle effects can be separated from data sets where they both occur at the same time.

Further studies on the incidence angle effect on intensity are also needed for ALS, particularly for validation and improving the accuracy of currently available methods and implementing these methods in practical applications. One option is to relate the backscatter cross section (see Equation (1)) to the cross section of the incoming beam and use the resulting backscattering coefficient as a calibration parameter. This approach has been recently suggested for full waveform ALS [5,6].

**Figure 6.** The  $K/R^2$  function (scaled to  $K/R^2 = 1$  at  $R = 12$  m) plotted over intensity vs. range data, all scaled to equal 1 at 12 m.



## 5. Conclusions

We have studied the range and incidence angle effects on the intensity measurement and radiometric calibration for different terrestrial laser scanners to establish a correction scheme for both of these effects. Knowing and correcting for these effects is essential, e.g., in stationary TLS from multiple directions or mobile applications, which are constantly increasing.

As the distance effect is strongly dependent on the instrument, the best correction scheme is based on a reference table, *i.e.*, reference measurement using an external target (also *cf.* [31]). Correction based on the LiDAR equation is possible, but it only works after 10–15 m distance for the instruments we studied and scaling with a constant may be necessary. Future research will show whether a physical explanation or a model is possible for the near-distance and other effects.

We also propose an empirical correction function for the incidence angle effect (see Equation (6)). A more detailed study is still needed to further investigate the role of surface parameters, such as surface roughness or grain size. If these parameters could be studied by means of incidence angle from TLS intensity data, it would greatly enhance the use of TLS in environmental applications.

## Acknowledgements

This study was financially supported by the Academy of Finland (projects “New techniques in active remote sensing: hyperspectral laser in environmental change detection”, “Towards improved characterization of map objects”, and “Modelling and applications of stochastic and regular surfaces in inverse problems”).

## References and Notes

1. Jelalian, A.V. *Laser Radar Systems*; Artech House: Norwood, NJ, USA, 1992; pp. 3-10.
2. Wagner, W.; Ullrich, A.; Ducic, V.; Melzer, T.; Studnicka, N. Gaussian decomposition and calibration of a novel small-footprint full-waveform digitising airborne laser scanner. *ISPRS J. Photogramm.* **2006**, *60*, 100-112.
3. Höfle, B.; Pfeifer, N. Correction of laser scanning intensity data: Data and model-driven approaches. *ISPRS J. Photogramm.* **2007**, *62*, 415-433.
4. Kaasalainen, S.; Hyypä, H.; Kukko, A.; Litkey, P.; Ahokas, E.; Hyypä, J.; Lehner, H.; Jaakkola, A.; Suomalainen, J.; Akujärvi, A.; Kaasalainen, M.; Pyysalo, U. Radiometric calibration of LIDAR intensity with commercially available reference targets. *IEEE Trans. Geosci. Remote Sens.* **2009**, *47*, 588-598.
5. Wagner, W. Radiometric calibration of small-footprint full-waveform airborne laser scanner measurements: Basic physical concepts. *ISPRS J. Photogramm.* **2010**, *65*, 505-513.
6. Lehner, H.; Briese, C. Radiometric Calibration of Full-Waveform Airborne Laser Scanning Data Based on Natural Surfaces. In *Proceedings of ISPRS Technical Commission VII Symposium, 100 Years ISPRS, Advancing Remote Sensing Science*, Vienna, Austria, 5–7 July 2010; In *IAPRS*; 2010; Volume 38, pp. 360-365.
7. Pfeifer, N.; Höfle, B.; Briese, C.; Rutzinger, M.; Haring, A. Analysis of the Backscattered Energy in Terrestrial Laser Scanning Data. In *Proceedings of ISPRS Congress*, Beijing, China, 7–11 July 2008; In *IAPRS*; 2008; Volume 37, pp. 1045-1052.
8. Béland, M.; Widlowski, J.-L.; Fournier, R.A.; Côté, J.-F.; Verstraete, M.M. Estimating leaf area distribution in savanna trees from terrestrial LiDAR measurements. *Agric. Forest Meteorol.* **2011**, *151*, 1252-1266.
9. Franceschi, M.; Teza, G.; Preto, N.; Pesci, A.; Galgaro, A.; Girardi, S. Discrimination between marls and limestones using intensity data from terrestrial laser scanner. *ISPRS J. Photogramm.* **2009**, *64*, 522-528.
10. Burton, D.; Dunlap, D.B.; Wood, L.J.; Flaig, P.P. Lidar intensity as a remote sensor of rock properties. *J. Sediment. Res.* **2011**, *81*, 339-347.
11. Nield, J.M.; Wiggs, G.F.S.; Squirrell, R.S. Aeolian sand strip mobility and protodune development on a drying beach: examining surface moisture and surface roughness patterns measured by terrestrial laser scanning. *Earth Surf. Proc. Land.* **2011**, *36*, 513-522.
12. Kaasalainen, S.; Kukko, A.; Lindroos, T.; Litkey, P.; Kaartinen, H.; Hyypä, J.; Ahokas, E. Brightness measurements and calibration with airborne and terrestrial laser scanners. *IEEE Trans. Geosci. Remote Sens.* **2008**, *46*, 528-534.

13. Kaasalainen, S.; Krooks, A.; Kukko, A.; Kaartinen, H. Radiometric calibration of terrestrial laser scanners with external reference targets. *Remote Sens.* **2009**, *1*, 144-158.
14. Balduzzi, M.A.F.; Van der Zande, D.; Stuckens, J.; Verstraeten, W.W.; Coppin, P. The properties of terrestrial laser system intensity for measuring leaf geometries: A case study with conference pear trees (*Pyrus Communis*). *Sensors* **2011**, *11*, 1657-1681.
15. Lichti, D.D. Modelling of Laser Scanner NIR Intensity for Multi-Spectral Point Cloud Classification. In *Proceedings of Optical 3D Measurement Techniques VI*, Zürich, Switzerland, 22–25 September 2003; pp. 282-289.
16. Eitel, J.U.H.; Vierling, L.A.; Long, D.S. Simultaneous measurements of plant structure and chlorophyll content in broadleaf saplings with a terrestrial laser scanner. *Remote Sens. Environ.* **2011**, *115*, 628-635.
17. Voegtle, T.; Wakaluk, S. Effects on the Measurements of the Terrestrial Laser Scanner HDS 6000 (Leica) Caused by Different Object Materials. In *Proceedings of Laserscanning 2009*, Paris, France, 1–2 September 2009; In *IAPRS*; 2009; Volume 38, pp. 68-74.
18. Soudarissanane, S.; Lindenbergh, R.; Menenti M.; Teunissen, P. Incidence Angle Influence on the Quality of Terrestrial Laser Scanning Points. In *Proceedings of Laserscanning 2009*, Paris, France, 1–2 September 2009; In *IAPRS*; 2009; Volume 38, pp. 83-88.
19. Pesci, A.; Teza, G. Effects of surface irregularities on intensity data from laser scanning: An experimental approach. *Ann. Geophys.* **2008**, *51*, 839-848.
20. Jaakkola, A.; Hyyppä, J.; Hyyppä, H.; Kukko, A. Retrieval algorithms for road surface modelling based on mobile mapping. *Sensors* **2008**, *8*, 5238-5249.
21. Alho, P.; Kukko, A.; Hyyppä, H.; Kaartinen, H.; Hyyppä, J.; Jaakkola, A. Application of boat-based laser scanning for river survey. *Earth Surf. Proc. Land.* **2009**, *34*, 1831-1838.
22. Kaasalainen, S.; Vain, A.; Krooks, A.; Kukko, A. Topographic and Distance Effects in Laser Scanner Intensity Correction. In *Proceedings of Laserscanning 2009*, Paris, France, 1–2 September 2009; In *IAPRS*; 2009; Volume 38, pp. 219-223.
23. Jutzi, B.; Gross, H. Normalization of LiDAR Intensity Data Based on Range and Surface Incidence Angle. In *Proceedings of Laserscanning 2009*, Paris, France, 1–2 September 2009; In *IAPRS*; 2009; Volume 38, pp. 213-218.
24. Lichti, D.D.; Spectral filtering and classification of terrestrial laser scanner point clouds. *Photogramm. Rec.* **2005**, *20*, 218-240.
25. Hodge, R.; Brasington, J.; Richards, K. *In situ* characterization of grain-scale fluvial morphology using terrestrial laser scanning. *Earth Surf. Proc. Land.* **2009**, *34*, 954-968.
26. Rees, W.G.; Arnold, N.S. Scale-dependent roughness of a glacier surface: Implications for radar backscatter and aerodynamic roughness modelling. *J. Glaciol.* **2006**, *52*, 214-222.
27. Egli, L.; Jonas, T.; Grünwald, T.; Schirmer, M.; Burlando, P. Dynamics of snow ablation in a small Alpine catchment observed by repeated terrestrial laser scans. *Hydrol. Process.* **2011**, in press.
28. Kukko, A.; Kaasalainen, S.; Litkey, P. Effect of incidence angle on laser scanner intensity and surface data. *Appl. Opt.* **2008**, *47*, 986-992.

29. Labsphere Inc. *Reflectance Materials and Coatings, Technical Guide*; Labsphere Inc.: North Sutton, NH, USA. Available online: <http://www.labsphere.com/uploads/technical-guides/a-guide-to-reflectance-materials-and-coatings.pdf> (accessed on 19 October 2011).
30. Jaakkola, A.; Kaasalainen, S.; Hyyppä, J.; Niittymäki, H.; Akujärvi, A. Intensity Calibration and Imaging with SwissRanger SR-3000 Range Camera. In *Proceedings of the ISPRS Congress Beijing 2008*, Beijing, China, 3–11 July 2008; In *IAPRS*; 2008; Volume 36, pp. 155-159.
31. Pfennigbauer, M.; Ullrich, A. Improving quality of laser scanning data acquisition through calibrated amplitude and pulse deviation measurement. *Proc. SPIE* **2010**, doi:10.1117/12.849641.
32. Hapke, B. *Theory of Reflectance and Emittance Spectroscopy*; Cambridge University Press: Cambridge, UK, 1993; p. 185.
33. Kaasalainen, S.; Kaasalainen, M.; Piironen, J. Ground reference for space remote sensing: Laboratory photometry of an asteroid model. *Astron. Astrophys.* **2005**, *440*, 1177-1182.
34. Kaasalainen, M.; Lamberg, L. Inverse problems of generalized projection operators. *Inverse Probl.* **2006**, *22*, 749-769.
35. Kaasalainen, S.; Ahokas, E.; Hyyppä, J.; Suomalainen, J. Study of surface brightness from backscattered laser intensity: Calibration of laser data. *IEEE Geosci. Remote Sens. Lett.* **2005**, *2*, 255-259.

© 2011 by the authors; licensee MDPI, Basel, Switzerland. This article is an open access article distributed under the terms and conditions of the Creative Commons Attribution license (<http://creativecommons.org/licenses/by/3.0/>).